American Mineralogist, Volume 68, pages 744–753, 1983

Phase characterization of synthetic amphiboles on the join Mn_x^{2+} Mg_{7-x} $[Si_8O_{22}]$ $(OH)_2$

WALTER V. MARESCH

Institut für Mineralogie
Ruhr-Universität Bochum, 463 Bochum, F.R. Germany

AND MICHAEL CZANK

Mineralogisch-Petrographisches Institut
Universität Kiel, Olshausenstr. 40–60, 2300 Kiel, F.R. Germany

Abstract

The crystal chemistry of synthetic amphibole solid solutions with nominal bulk compositions between $Mn_{0.3}Mg_{6.7}[Si_8O_{22}]$ $(OH)_2$ and $Mn_{2.3}$ $Mg_{4.7}[Si_8O_{22}]$ $(OH)_2$ has been investigated. Synthesis runs carried out at 750°C/2000 bar ($Mn_{0.3}$ to $Mn_{1.8}$) and 650°C/6000 bar ($Mn_{2.0}$ to $Mn_{2.3}$) led to essentially single-phase products. In contrast to natural amphiboles of similar composition, X-ray and optical properties that reflect long-range symmetry are consistent with space group *Pnma*. The cell volume and mean refractive index generally increase with increasing Mn-substitution, but *a* and *b* lattice parameter variation is not a simple function of Mn-content. HRTEM studies reveal abundant chain multiplicity (chain-width) and chain arrangement (stacking) faults. The Mn-bearing analogs of chesterite and jimthompsonite, as well as other statistically significant multiple chain combinations, have been noted. The observed consistent and reproducible nature of structural and compositional inhomogeneity suggests that many synthetic amphiboles are poor experimental analogs of their natural counterparts.

Introduction

Members of the Fe–Mg–Mn-amphibole group, such as anthophyllite, gedrite, grunerite, cummingtonite, tirodite and dannemorite (Leake, 1978), are important phases in many natural assemblages that are relatively poor in Ca. A knowledge of their phase relations is therefore of considerable importance. The group also contains some of the chemically simplest amphibole forms known and encompasses three (*C2/m*, *Pnma*, $P2_1/m$) of the four structural types so far found in nature (Hawthorne, 1981). Detailed study of this group should therefore be particularly fruitful in elucidating the basic constraints governing amphibole crystal chemistry.

Nevertheless, the stability and compositional relationships among the three space group possibilities are still not well understood (*e.g.*, Ross *et al.*, 1969). Moreover, these amphiboles have proven to be particularly recalcitrant subjects during experimental investigations (see, for example, the discussion of Day and Halbach, 1979, for magnesio-anthophyllite, $Mg_7[Si_8O_{22}](OH)_2$). Forbes (1971) reported the first synthesis of grunerite, Fe_7^{2+} $[Si_8O_{22}](OH)_2$, and discussed the experimental difficulties of its synthesis. Intermediate compositions between these end-members have been experimentally studied by Hinrichsen (1967), Cameron (1975), Ravior and Hinrichsen (1975) and in considerable detail by Popp *et al.* (1976). Popp *et al.* noted, however, that their synthetic products differed in several important respects from the natural counterparts and concluded that the synthetic products possess a "structure type unlike any known amphibole."

To our knowledge, no explicit experimental data are available on the join magnesio-anthophyllite–tirodite ($Mn_2Mg_5[Si_8O_{22}](OH)_2$), although Ito (1972) has observed "Mn-cummingtonite" during synthesis runs on the join $MgSiO_3$–$MnSiO_3$.

The present report is a summary of experimental results for amphibole compositions $Mn_x^{2+}Mg_{7-x}[Si_8O_{22}]$ $(OH)_2$, where x varies between 0.3 and 2.3, that have been obtained over a number of years during studies of the system MnO–MgO–SiO_2–H_2O. The crystal-chemical characteristics of the synthetic products diverge markedly and reproducibly from their natural analogs, making it clear that before an adequate phase characterization of synthetic amphiboles has been achieved, the phase relations deduced using such products in further experiments may be subject to considerable uncertainty.

Experimental procedure

All runs were performed in standard, cold-seal pressure vessels (38 × 250 mm, 6 mm bore) placed in horizontal

0003–004X/83/0708–0744$02.00

split furnaces. Temperature was controlled and continuously monitored with chromel-alumel thermocouples. All autoclaves were routinely calibrated internally with three thermocouples distributed over the capsule length. Gradients were less than 3–5°C and total temperature uncertainties are estimated to be less than ±10°C. Pressures were determined using Bourdon-type manometers and strain-gauge transducer systems. Experimental uncertainty is less than ±50 bar.

Starting materials were gels, prepared according to the method of Hamilton and Henderson (1968), with manganese metal (Schuchardt, MA 055), magnesium metal (Schuchardt, MA 011) and tetraethylorthosilicate. The composition of the starting material has been corroborated by chemical analysis (Table 1).

The resulting oxidized, dark-brown powder was sealed into Pt-capsules with approximately 10 wt.% doubly distilled water. The seal was checked for leakage before and after each run. In accordance with similar observations by Hsu (1968), Dasgupta *et al.* (1974), and Maresch and Mottana (1976), the inherent f_{O_2} of the nickel alloy pressure vessel, in conjunction with water as pressure medium, was found to be suitable for a rapid reduction to and retention of Mn in the divalent state. No additional buffering techniques were necessary.

Favorable experimental conditions for high amphibole yields are 750°C/2000 bar up to and including an Mn-content of $Mn_{1.8}$ (for short-form designation of compositions see Table 1). Beyond this composition a three-phase field of quartz + pyroxene + amphibole is encountered and conditions were changed to 650°C/6000 bar, where the amphiboles $Mn_{2.0}$ and $Mn_{2.3}$ could be synthesized.

For lattice constants, powder X-ray patterns were obtained on a Philips X-ray powder diffractometer, which was run at 50 kV, 30 mA, with 1/8° 2θ/min scanning speed, 300 mm/hr chart speed, 1/2°–0.2 mm–1/2° slit system, 2-second time constant, and Ni-filtered Cu$K\alpha$ radiation. The internal standard was Si (SRM 640, Nat'l Bureau of Standards, Washington). All reflection peaks were measured as close to the maximum as possible (see Wright and Stewart, 1968, p. 41), and only the Cu$K\alpha_1$ wavelength was used in the refinement. Values from two scans between 9° and 80° 2θ were averaged.

Indexing was carried out by comparison with the calculated powder patterns of Borg and Smith (1969) for anthophyllite (*Pnma*), Mn-cummingtonite (*C2/m*), tirodite ($P2_1/m$), and protoamphibole (*Pnmn*). Lattice constants were then refined with the Evans *et al.* (1963) program, but only fixed, unequivocally indexable reflections were employed.

Description of synthetic phases

No amphibole was obtained for bulk compositions $Mn_{0.3}$ and $Mn_{0.6}$. On the other hand, a gel with considerable SiO_2 excess, but projecting to $Mn_{0.3}$ from SiO_2, easily yielded the two-phase assemblage amphibole + quartz. This material has been included in the series under study. Work at present underway on the kinetics of amphibole crystallization in the MnO–MgO–SiO_2–H_2O system has shown that the nature of the starting material is a critical factor for successful amphibole synthesis. Partial crystallization of manganiferous pyroxene from the gel can be easily incurred during the burning-off phase of organic solvents in the gel-preparation process. In such cases amphibole has not been observed to nucleate during subsequent hydrothermal treatment. In successful amphibole synthesis runs, metastable talc crystallizes rapidly from the amorphous gel and apparently forms the substrate for amphibole nucleation and growth. Analogous observations have been reported by Greenwood (1963) from the Mn-free system. It thus appears that the amphibole microstructures to be described in this paper may not be due to primary growth, but are instead inherited from the reaction of the sheet silicate talc to the chain silicate amphibole.

Table 1. Data on starting material and synthesis conditions

Condensed Starting Material[+]	Analysis as Formula ions[++] Mn	Mg	Si	Synthesis Conditions (°C/bar)	Aggregate[++++] Run time (h)	Maximum Crystal size (μm)
$Mn^{+++}_{0.3}$	0.30	6.70	8[+++]	750/2000	4464	15 x 1.5 x 1.5
$Mn_{0.9}$	0.90	6.02	8.04	750/2000	1752	7 x .75 x .75
$Mn_{1.0}$	no analysis			750/2000	2630	5 x 0.5 x 0.5
$Mn_{1.2}$	1.21	5.78	8.01	750/2000	3672	10 x 1.0 x 1.0
$Mn_{1.5}$	1.49	5.40	8.05	750/2000	2630	7 x 0.5 x 0.5
$Mn_{1.8}$	1.80	5.14	8.03	750/2000 650/6000	672 1008	5 x 0.5 x 0.5
$Mn_{2.0}$	2.01	5.15	7.92	650/6000	3773	10 x 0.5 x 0.5
$Mn_{2.3}$	2.28	4.55	8.09	650/6000	1344	5 x 0.5 x 0.5

[+] Mn_x represents $Mn^{2+}_x Mg_{7-x} Si_8 O_{23}$

[++] analyst G. Werding, Bochum; formula on basis of 23 x (O)

[+++] projected from composition with excess SiO_2; actual value: Mn = 0.22; Mg = 4.94; Si = 8.92

[++++] runs were repeatedly interrupted and charge reground

In all products (except $Mn_{0.3}$, as noted above), routine X-ray diffraction indicated no additional phases. Optical examination revealed scattered laths of euhedral pyroxene and anhedral, globular glass and/or quartz (often interstitial to the amphibole fibers). The latter appear to be mainly quench products from the gas phase. Traces of MnO were noted for $Mn_{1.8}$ and $Mn_{2.3}$. The proportion of non-amphibole components in the products is estimated to be significantly less than 5%.

The synthetic amphibole is colorless in grain mounts, except for $Mn_{2.3}$, where a greenish tinge has been noted, and has a typically fibrous habit. The maximum length of the crystallites varies from 15 μm to less than 5 μm (Table 1). Typical length/width ratios are approximately 10/1. Extinction is parallel.

For two of the amphibole products, water analyses using a coulometric method (see Johannes and Schreyer,

1981) were carried out. Composition $Mn_{0.9}$ yielded 2.33±0.15 wt.% H_2O (theor. 2.23 wt.%), while for $Mn_{1.8}$ 2.14±0.15 wt.% was determined (theor. 2.15 wt.%). The stated uncertainty represents two estimated standard deviations. The agreement between the bulk H_2O content and the theoretically expected value is excellent.

X-ray diffraction results

As in most hydrothermal studies involving amphibole, the size of the available crystallites precludes single crystal techniques, so that bulk powder diffraction methods must be used. The quality of the powder diffractograms is not high, and peak broadening is common. The best pattern was obtained for $Mn_{0.3}$ (SiO_2 excess!), where 18 reflections were suitable for the refinement, of which 8 yielded data on the c parameter. Conversely, for $Mn_{1.8}$ only 9 peaks could be measured with sufficient accuracy, and for only two of these was $l \neq 0$. The number of reflections used and the results obtained for space group *Pnma* are summarized in Table 2.

Of the known amphibole space groups, *Pnma* appears to fit the bulk amphibole product best. The observed parallel optical extinction of single amphibole fibers speaks against the monoclinic forms $C2/m$ and $P2_1/m$ (natural monoclinic amphiboles of similar compositions have $Z \wedge c > 15°$, *e.g.*, Klein, 1964), as does the existence of X-ray reflections at approximately 24.3°, 31.5°, and 35.2° 2θ Cu$K\alpha$. (The electron microscopic studies also show that an 18.6Å repeat in the a direction predominates; monoclinic $P2_1/m$ and $C2/m$, as well as orthorhombic *Pnmn*, have approximately 9.5Å repeats). A relatively prominent X-ray reflection exists, which corresponds to 4.7Å and is perfectly indexable as (400) in *Pnma*, but should have negligible calculated intensity according to Borg and Smith (1969).

The lattice parameters obtained are plotted in Figure 1, along with data on natural amphiboles of similar composition. As expected, the unit cell volume and the c-parameter generally increase with Mn substitution. Available data for synthetic magnesio-anthophyllite do not fit the observed trends. In the a- and b-parameters there is also an overall increase with increasing Mn, although scatter is significant. $Mn_{0.3}$ (the amphibole coexisting with quartz), although yielding the best X-ray diffractogram and containing the fewest structural defects (see next section), shows a particularly large a-parameter deviation.

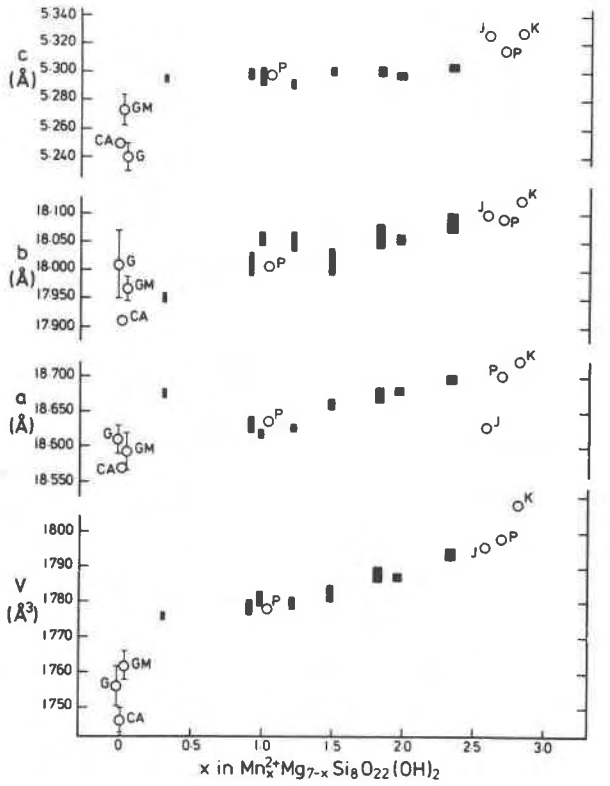

Fig. 1. Unit cell parameters of synthetic orthoamphiboles. Solid rectangles: this study. Data on synthetic magnesio-anthopyllite: CA (Chernosky and Autio, 1979), G (Greenwood, 1963) and GM (Greenwood's data reindexed in analogy to present amphiboles). Natural clinoamphiboles: P (Papike *et al.*, 1969), J (Jaffe *et al.*, 1961), K (Kombat Mine, S. W. Africa, unpubl. author data). Size of symbol ≥ estimated uncertainties.

Table 2. Unit cell data for Mn_x^{2+} $Mg_{7-x}[Si_8O_{22}](OH)_2$ in space group *Pnma*

x	V(Å³)⁺	a(Å)⁺	b(Å)⁺	c(Å)⁺	N⁺⁺
0.3	1775.8(1.0)	18.677(6)	17.954(8)	5.296(2)	18(8)
0.9	1778.4(1.9)	18.631(11)	18.012(21)	5.299(4)	13(5)
1.0	1780.8)1.9)	18.619(4)	18.054(11)	5.298(5)	13(2)
1.2	1779.3(1.4)	18.628(4)	18.051(16)	5.292(3)	12(2)
1.5	1782.1(1.9)	18.661(6)	18.017(21)	5.301(2)	13(3)
1.8	1787.9(1.9)	18.674(9)	18.061(20)	5.301(3)	9(2)
2.0	1786.9(1.0)	18.681(4)	18.056(7)	5.298(2)	13(2)
2.3	1793.6(1.5)	18.697(5)	18.086(16)	5.304(2)	11(2)

⁺ numbers in parentheses are one standard deviation, as given by least squares refinement

⁺⁺ number of reflections used in refinement; value in brackets is number of reflections where $l \neq 0$

A $P2_1/m$ tirodite (nomenclature of Leake, 1978) with negligible Fe^{2+}, described by Papike *et al.* (1969), is the best known natural example of the present composition series. It corresponds to $Mn_{1.03}$. The unit cells are compared in Figure 1 by doubling the cell volume of the tirodite and equating $2a\sin\beta$ with the orthorhombic a. The agreement is excellent. Three monoclinic tirodites with $Mn_{2.6}$ to $Mn_{2.8}$ are also in fair agreement, although these contain about 10% Fe^{2+}.

These results are analogous to those of Popp *et al.* (1976), who found on the join $Mg_7[Si_8O_{22}](OH)_2$–Fe_7^{2+} $[Si_8O_{22}](OH)_2$ that (1) orthorhombic amphiboles were synthesized for compositions that are monoclinic in na-

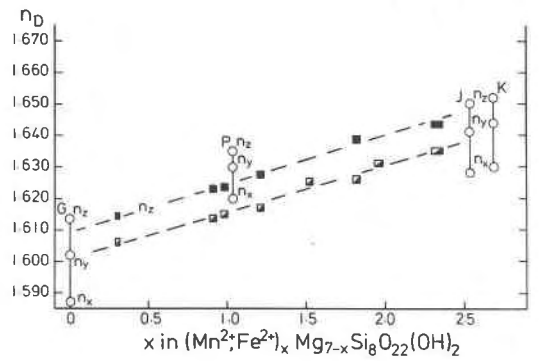

Fig. 2. Mean refractive index (half-filled rectangles) and $n(Z)$ (solid rectangles) for synthetic amphiboles of present study (size of symbol reflects experimental uncertainty), compared to natural monoclinic, manganoan cummingtonite. G, J, P, K as in Fig. 1 (optical data for P from Segeler, 1961).

ture, and (2) the cell volumes of synthetic orthorhombic products are in better agreement with natural monoclinic rather than natural orthorhombic analogs.

Refractive index

Bulk refractive indices, and where possible $n(Z)$ (which is parallel to c), were measured using λT-variation methods. To facilitate better recognition of the match between amphibole and Cargille immersion oils, the phase contrast mode was employed.

The results are displayed in Figure 2, compared to Greenwood's (1963) magnesio-anthophyllite data and several natural monoclinic tirodites. The present data set shows the expected increase in refractive index with Mn-substitution. The index $n(Z)$ agrees well with Mn-rich tirodites (J, K of Fig. 2), but poorly with Segeler's (1961) determination on a $P2_1/m$ tirodite (P) and Greenwood's value (G) for synthetic magnesio-anthophyllite.

High resolution electron microscopy

The electron microscope used was a Philips EM 400, operated at 100 kV and provided with a tilting stage. Specimens were ground and deposited on perforated carbon films. The results of a detailed HRTEM survey are discussed extensively elsewhere (Czank and Maresch, in prep.); a short overview is given here.

In contrast to a natural monoclinic tirodite from Kombat (S. W. Africa), which was studied for comparison, the synthetic products show a high degree of structural disorder, with disorder generally increasing with decreasing Mn-substitution. According to visual estimates, about one third of the overall crystal volume is structurally disordered. However, quantitative estimates of the type and abundance of the specific defect types making up the disordered structure are not feasible. Time studies have shown that defects present after 50–100 hours remain virtually unchanged for experiment durations of 10.000 hours or more.

Two types of planar faults have been commonly observed: (1) parallel (010): faults caused by incorporation of chains having multiplicities $m \neq 2$ into the ordered sequence of double chains (chain multiplicity faults)[1], and (2) parallel (100): faults in the periodic packing or arrangement of chains (chain arrangement faults)[1].

Because of the elongated tabular habit and typical (210) orthoamphibole cleavage, the amphibole crystals tend to be oriented mainly with a^* nearly parallel to the electron beam. Only in a few cases could crystals be oriented with a^* perpendicular to the beam, as is required for imaging the (100) lattice fringes. In such crystals, various $d(100)$-spacings are observed, indicating a high incidence of chain arrangement faults (Fig. 3a). Stacking schemes representative of known monoclinic cells ($d(100) \approx 9.3$Å; as in $C2/m$, $P2_1/m$, $P2/a$) as well as orthorhombic $Pnmn$ ($d(100) \approx 9.3$Å) and $Pnma$ ($d(100) \approx 18.6$Å) can be observed, but other variants also occur ($d(100) \approx 13.95$, 23.25, or 27.9Å), pointing to as yet unidentified chain arrangements. Due to inferior contrast in these cases, resulting from the crystal thickness in this orientation, it was not possible to characterize these faults in detail.

Since most of the crystals were oriented with their b^* nearly perpendicular to the beam, and in this orientation were thin enough for HRTEM study, a detailed survey of chain multiplicity faults could be carried out. The multiplicity m, *i.e.*, the number of subchains, of a multiple chain can be deduced from the $d(0k0)$-values in the lattice fringe images. A fringe distance of 9.0Å corresponds to the normal double chain ($m = 2$). Variation of m by 1 changes the $d(0k0)$-value by 4.5Å. Various chain multiplicity faults were found which consist of multiple chains with $m = 3, 4, 5, 6$ and up to 10 (Fig. 3b). Slabs composed only of triple chains ($m = 3$), as in Fig. 3c, or alternating double ($m = 2$) and triple ($m = 3$) chains (Fig. 3d), analogous to jimthompsonite and chesterite (Veblen and Burnham, 1978a, 1978b), respectively, occur quite frequently. Slabs of other multiple chain combinations or

[1] Tetrahedral chains, and in general any other types of chains, are characterized by their *periodicity p* and their *multiplicity m*. Periodicity p is the number of tetrahedra within the repeat unit of a single chain (or subchain). For pyriboles $p = 2$. Multiplicity m is the number of subchains that are linked to form a multiple chain. If an ordered sequence of multiple chains is interrupted by a chain with "wrong" multiplicity, the corresponding error is called a *chain multiplicity error*. A two-dimensional arrangement of chain multiplicity errors is called a *chain multiplicity fault* (Czank and Liebau, 1980). The term *chain width error* has been introduced for such faults in biopyriboles (Veblen and Buseck, 1979). The term *chain arrangement fault* has been suggested (Czank and Liebau, 1980) as a general term covering all known types of planar faults in chain structures, where the chain characters p and m remain unchanged (*e.g.*, stacking fault, twin boundary, planar antiphase boundary). In particular, it may be used if the specific structure of the fault has not been determined.

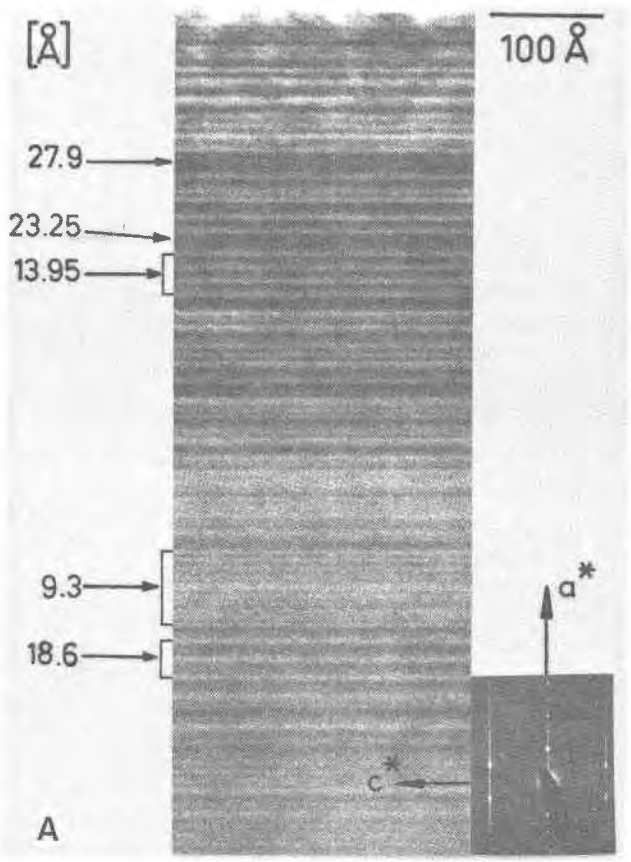
[Å]
100 Å
27.9
23.25
13.95
9.3
18.6
a*
c*
A

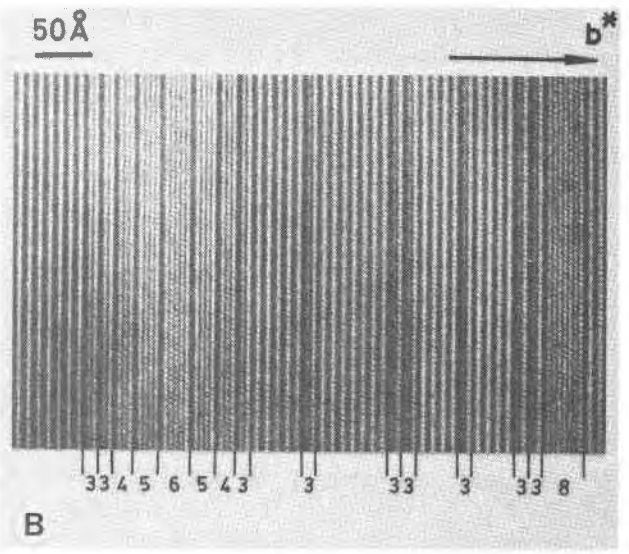
50 Å
b*
3 3 4 5 6 5 4 3 3 3 3 3 8
B

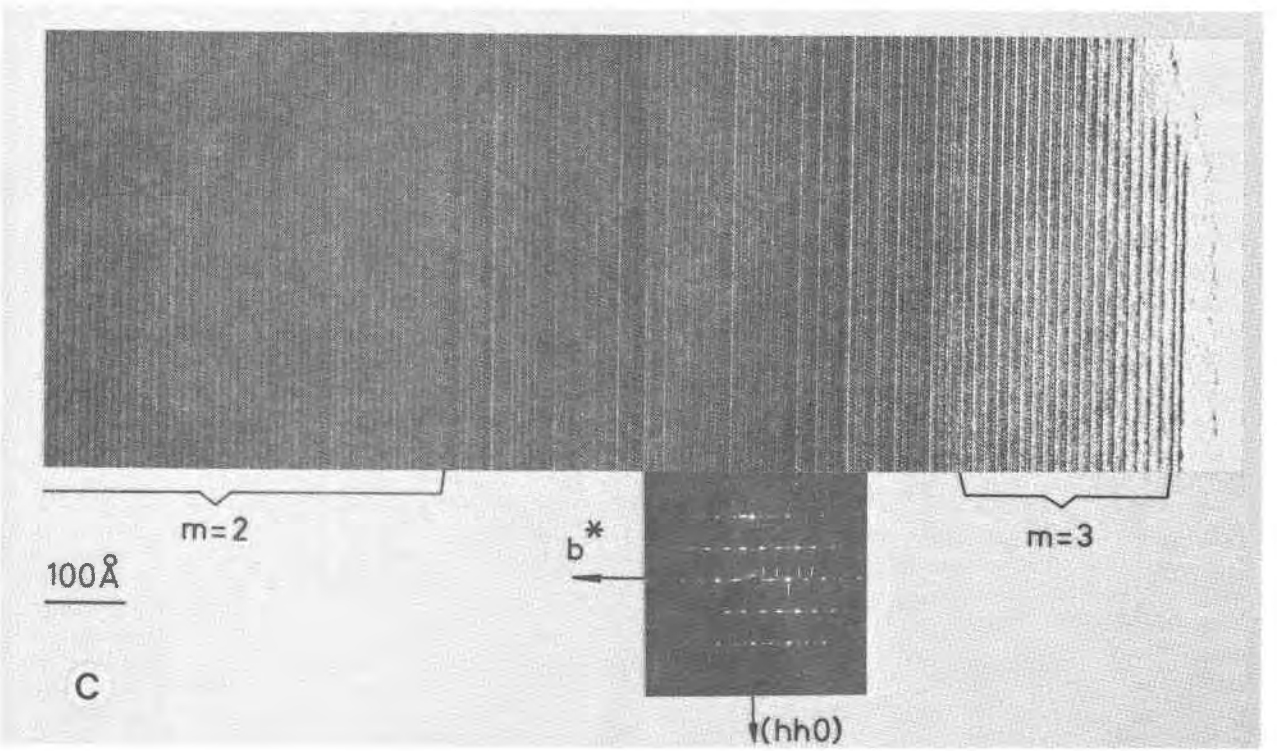
m=2
m=3
100 Å
b*
(hh0)
C

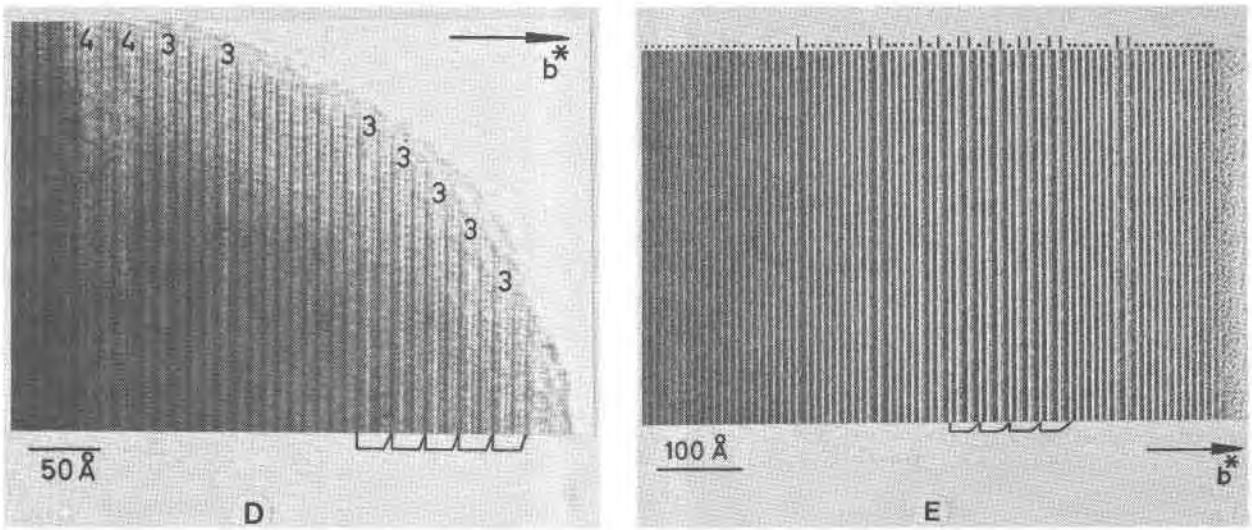

Fig. 3. Examples of structural defects in synthetic $Mn_xMg_{7-x}[Si_8O_{22}](OH)_2$: (a) ($h00$) lattice fringe image containing various chain arrangement (stacking) faults. Some of possible ($h00$) spacings are indicated; brackets delineate intervals with same stacking mode (inferior contrast due to crystal thickness). (b–e) ($0k0$) lattice fringe images containing various chain multiplicity faults. (b) randomly distributed chain multiplicity faults labelled with the corresponding multiplicity m; for unlabelled intervals $m = 2$. (c) homogeneous regions of double-chain or ideal amphibole (left) and triple-chain or jimthompsonite-like structure (right), separated by interval of randomly distributed chain multiplicity faults. Small bars in diffraction pattern indicate diffraction spots corresponding to triple-chain structure. (d) chain multiplicity faults with indicated m; double chains are not labelled; brackets mark triple-double unit of chesterite-like slab. (e) slab of triple-triple-double chain structure indicated by brackets; bars mark triple chains, dots indicate double chains.

polysomes, such as double–triple–triple (in short form: 233), as in Figure 3e, or 223, 2223, 224, 234 and even more complex are also observed a number of times.

Within a given slab a certain variant may be repeated only a few times, so that the application of the probability test for random occurrence proposed by Veblen and Buseck (1979) results in values greater than the limit ($p = 0.001$) chosen by them (for 233 in Fig. 3e, $p = 0.0119$). According to Veblen and Buseck, such combinations should be considered to be statistically insignificant. However, since for certain multiple chain combinations *several* such slabs are observed, the probability test requires a further component. Such probability calculations are complex and necessitate consideration of the total number of observed multiple chains. A more detailed discussion will be given elsewhere (Czank and Maresch, in prep.).

Discussion

Figure 4 summarizes the compositional limits of space groups observed in nature for the Fe–Mg–Mn amphibole group. The compositional region of $P2_1/m$ determinations is also one of overlapping *Pnma* and *C2/m* occurrence. The mutual relationships among these three structure types are still problematical, although Sueno *et al.* (1972) have shown that Fe^{2+}-free, natural $P2_1/m$ tirodite can be converted to the *C2/m* space group by heating above 100°C. As suggested by Ross *et al.* (1969), the overlap

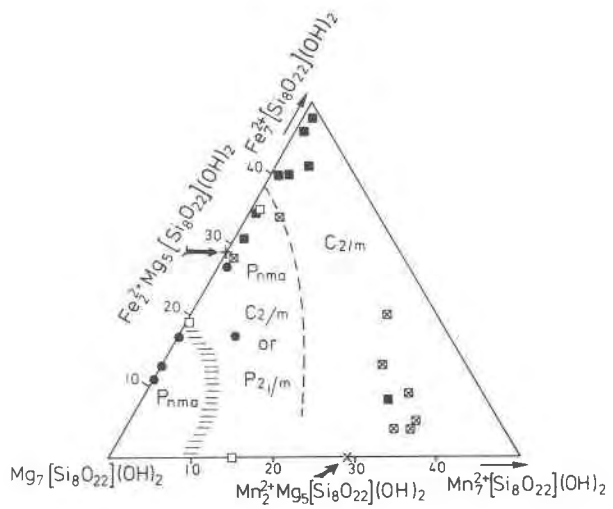

Fig. 4. The amphibole compositional plane $(Mg,Fe^{2+},Mn^{2+})_7[Si_8O_{22}](OH)_2$, outlining compositional limits (atomic percent) of space groups observed in nature. Solid circles: *Pnma*; solid squares: *C2/m*; open squares: $P2_1/m$; squares with cross: undifferentiated monoclinic. Only amphiboles with (half unit cell) $Mg + Fe^{2+} + Mn^{2+} > 6.5$, $Al_{total} < 0.3$, $Ca < 0.3$, and $Na < 0.1$ have been considered. Data from Johannsen (1930), Jaffe *et al.*, (1961), Lindemann (1964), Klein (1964, 1966), Kisch (1969), Seifert and Virgo (1974), Immega and Klein (1976), Peters *et al.*, (1977), Stephenson and Hensel (1979), Hawthorne *et al.*, (1980), and unpublished author data.

region may mark a compositional field where *P*- and *T*-dependent inversion from high-*T* *C*2/*m* to low-*T* *Pnma* should occur. This transformation, however, requires restacking of amphibole chains. Instead, a merely displacive transformation to metastable $P2_1/m$ takes place. Thus, the overlap region may be due mainly to kinetic factors. In any case, Figure 4 shows that monoclinic forms should be expected beyond 10–20 mol% (Fe, Mn)-endmember. Yet the present experimental results indicate overall orthorhombic symmetry up to 33 mol% Mn-endmember on the Fe^{2+}-free join.

Figure 5 is a summary diagram of unit cell data pertinent to Figure 1. Several features are noteworthy:

(1) The *b*-parameters of all synthetic and natural forms, whether orthorhombic or monoclinic, are generally consistent with each other. The effects of Mn^{2+} and Fe^{2+} substitution are qualitatively similar.

(2) For cell volumes and *c*-parameters, synthetic orthorhombic (Mg,Fe^{2+},Mn)-amphiboles conform to natural *monoclinic* values. Again, the qualitative effects of Fe^{2+} and Mn^{2+} substitution are similar. Synthetic, orthorhombic, endmember $Mg_7[Si_8O_{22}](OH)_2$ and natural orthorhombic (Mg,Fe^{2+})-amphiboles are consistent with each other, but are markedly lower in *c* and *V* than the former group.

(3) The largest variations occur in the *a*-parameter. Natural monoclinic and orthorhombic (Mg,Fe^{2+})- modifications are generally similar, while Mn^{2+}- introduction leads to significantly higher *a* in both the synthetic orthorhombic and the natural monoclinic forms.

Figure 5 is difficult to interpret on a crystal-chemical basis, because a number of factors may influence the distribution shown. The discrepancy in unit cell volume between synthetic and natural, orthorhombic, Fe–Mg-amphiboles has been discussed in detail by Popp *et al.* (1976), although a convincing explanation was not found. Our data on Mn–Mg-amphiboles do not resolve this problem. Nevertheless, there exists the plausible possibility that structural units (tetrahedral layers) of *C*2/*m* type could be randomly oriented with respect to the direction of c/3 stagger (see Hawthorne, 1981, p. 24), so that, on the average, a *Pnma*-like structure with a

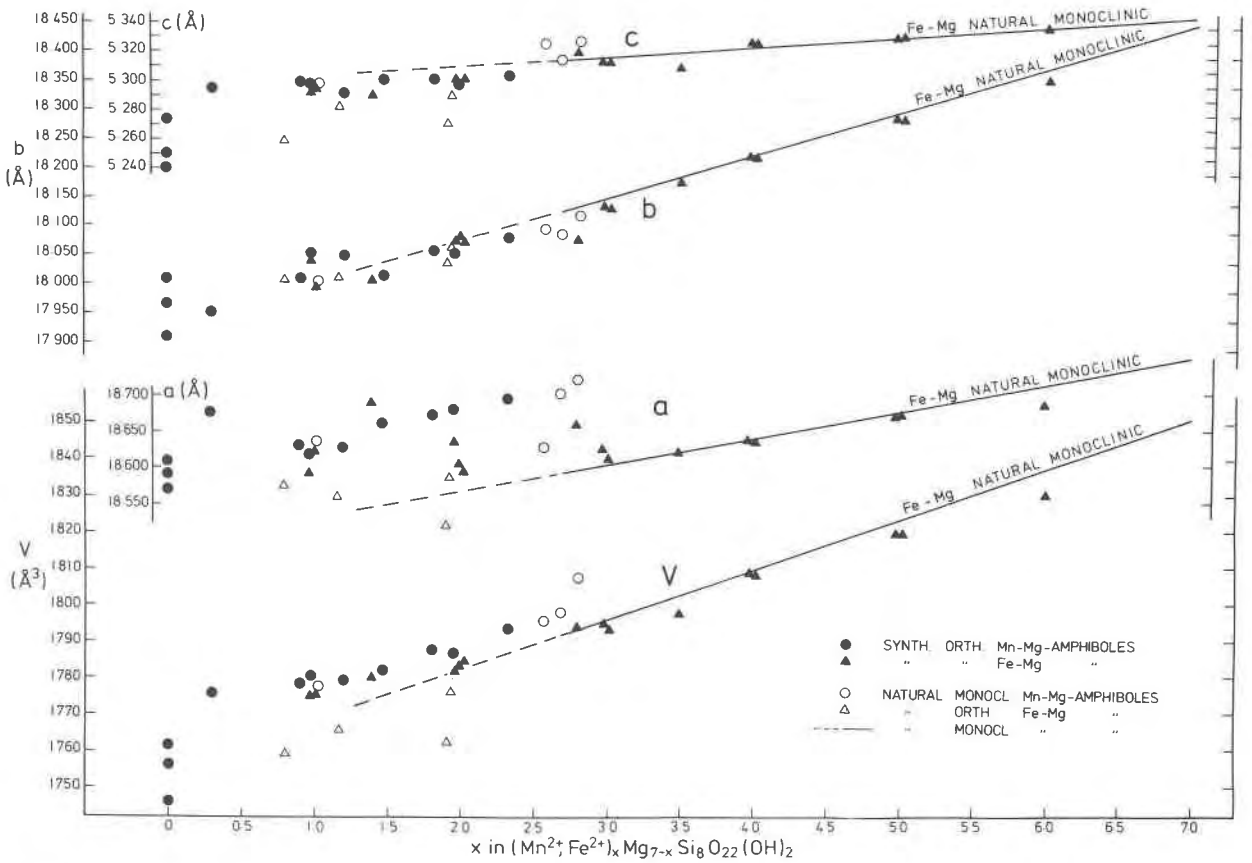

Fig. 5. Comparison of unit cell data of Fig. 1 with corresponding values for Mg–Fe-amphiboles. Data from Cameron (1975), Ravior and Hinrichsen (1975), Popp *et al.*, (1976) for synthetic forms, as well as Johannsen (1930), Lindemann (1964), Finger (1970), Seifert and Virgo (1974), and Veblen and Burnham (1978a) for natural orthorhombic examples. Regression curves from Klein and Waldbaum (1967), extrapolated on basis of value of Kisch (1969). $V_{orth} = 2 \cdot V_{mon}$; $a_{orth} = 2 \cdot a \cdot \sin\beta_{mon}$.

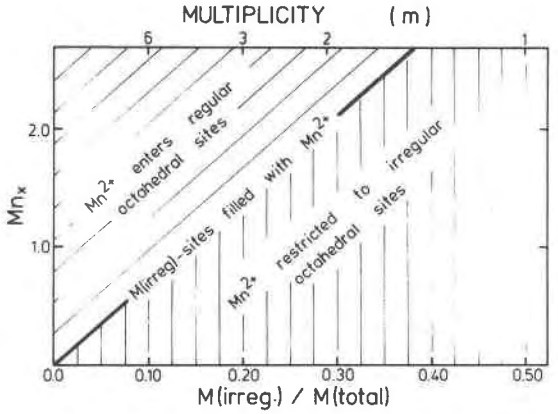

Fig. 6. Saturation of irregular octahedral sites with Mn^{2+} as function of bulk composition Mn_x, which represents $Mn_xMg_{7-x}[Si_8O_{22}](OH)_2$, and chain-silicate multiplicity m. Complete Mn^{2+}-preference for the irregular sites is assumed.

+ + – – stagger sequence in the a-direction could result. Thus, despite an ostensibly *Pnma* symmetry, the basic structure could be of monoclinic *C2/m* type. Possible evidence in favor of significant disorder in chain stacking is the prominent X-ray reflection at 4.7Å, as noted in a previous section, which mirrors the arrangement of octahedral layers in the a-direction. Whereas in ordered structures this X-ray reflection is weak (*e.g. C2/m*) or entirely absent (*e.g., Pnma*), it could be enhanced by structural disorder.

Popp *et al.* noted that the effects of varying degrees of Mg/Fe^{2+} ordering within the M-sites are too small to cause volume discrepancies of the magnitude evident in Figure 5. Such ordering effects might be expected to be greater for Mn^{2+}–Mg amphiboles, however, because of a greater difference in ionic radius. In addition, the presence of chain multiplicity faults changes the overall ratio of site types present (*e.g.*, Veblen, 1981). In natural amphiboles of the Fe–Mg–Mn group, the observed preference in the irregular M(4) site is $Mn^{2+} > Fe^{2+} > Mg$. In a structurally ideal, ordered amphibole, the M(4) site would be filled with Mn^{2+} when the composition reaches $Mn_2Mg_5[Si_8O_{22}](OH)_2$ (see Fig. 6). Only in product $Mn_{2.3}$ need Mn^{2+} enter the regular octahedral sites. However, as demonstrated in Figure 6, the Mn_x of saturation with Mn^{2+} decreases as the incidence and m of chain multiplicity faults increases. In short, both disordering processes as well as the presence of structural defects apparently cause entry of the larger Mn^{2+} cation into the smaller octahedral sites. Although the state of cation ordering in the synthetic products is unknown, and a statistically sound "average" defect structure cannot be defined, it does indeed appear that no significant differences exist in the lattice constant trends of the synthetic products and their natural counterparts (Fig. 1 and 5). Of the latter, at least those labelled "P" and "K" in Figure 1 may be confidently assumed to be ordered with respect to cation distribution and to be relatively free of structural defects (Papike *et al.*, 1969; Czank and Maresch, in prep.).

It is noteworthy that, while Mn^{2+} and Fe^{2+} substitution in the natural samples has approximately the same effect on b, this is not true for the parameter a. On the logical assumption that both Fe^{2+} and Mn^{2+} are respectively ordered into the M(4) site, this must mean that Mn^{2+} substitution into M(4) has a particularly strong influence on the stacking of tetrahedral chains in the a-direction.

Structural disorder implies chemical inhomogeneity in the structurally disordered amphibole product, because $Si/(Mn^{2+} + Mg)$ of multiple-chain polysomes increases with m, the number of subchains (Fig. 7). In addition, the bulk product must become SiO_2-richer, because *single*-chain multiplicity faults with *lower* $Si/(Mn^{2+} + Mg)$ are almost non-existent (see also Veblen and Buseck, 1981). At constant, condensed bulk composition, additional phases with $Si/(Mn^{2+} + Mg)$ smaller than in theoretical amphibole must be present for compensation. In the present case, pyroxene is the likely choice.

Theoretically, the pyroxene content of the product assemblage should be proportional to the incidence of chain multiplicity faults (*i.e.*, to the shift in overall SiO_2-content) and thus might be considered useful as a relative *measure* of the structural disorder. However, this approach appears impracticable. Figure 7 illustrates that the analytical uncertainties in the bulk SiO_2 content are too large in comparison to the SiO_2 differences between multiple-chain polysomes. An application of the lever rule (pyroxene composition:bulk composition:disor-

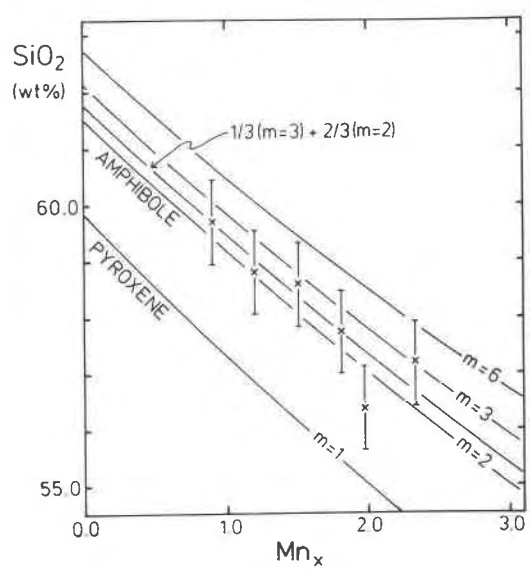

Fig. 7. Variation of calculated SiO_2 content with bulk composition Mn_x, which represents $Mn_xMg_{7-x}[Si_8O_{22}](OH)_2$, and chain-silicate multiplicity m. Starting material of present study indicated by crosses and error bars (for discussion see text).

dered amphibole composition) is unrealistic. Further complications arise from the indeterminate, but not insignificant, amount of SiO_2 preferentially leached into the vapor phase, thus effectively reducing the condensed bulk composition in SiO_2.

The salient feature arising from these considerations is that pyroxene should be a common and reasonably plentiful product phase. For instance, a disordered amphibole product composed of two parts double chains and one part triple chains requires, disregarding SiO_2 leaching, 13% pyroxene by weight in the run product, regardless of the Mn^{2+}/Mg ratio. SiO_2 leaching and chains with $m > 3$ will increase this proportion. Such concentrations of pyroxene are not observed. A consideration of the H_2O budget also yields unexpected results (Fig. 8). Whereas multiplicity faults should increase the bulk water content, the two available H_2O analyses are entirely in accord with ideal amphibole.

It appears that the synthetic products analyzed reveal a number of features that are not compatible with simple "mixing" of ideal double chains and ideal wider-chain polysomes. Explanations are at present speculative. The absence of larger amounts of pyroxene in the run products could theoretically be explained by a cation excess in the wide-chain defects, such as the partial introduction of Mn^{2+} and/or Mg into the enlarged "A-site," necessarily in conjunction with OH^-, in chemical analogy to chlorite. Although Mn^{2+} or Mg would not normally be expected to reside in such a large distorted site, it is noteworthy that Li, which has a comparable ionic radius, appears to be able to occupy the A-site in synthetic orthorhombic amphiboles (Gibbs, 1969; Maresch and Langer, 1976). The bulk water content of the chain silicate could be affected by substitutions such as $Mn^{3+} + O^{2-} \rightarrow Mn^{2+} + OH^-$, or $O^{2-} \rightarrow 2OH^-$. The bulk chemical effects observed will be the sum of all such processes. Selected area analyses of considerable precision and spectroscopic studies are needed to isolate possible substitution mechanisms.

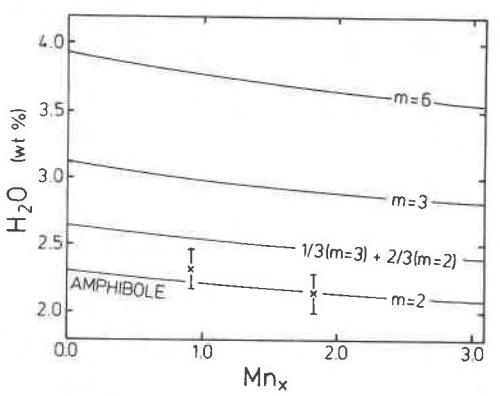

Fig. 8. Variation of calculated H_2O content with bulk composition Mn_x, which represents $Mn_xMg_{7-x}[Si_8O_{22}](OH)_2$, and chain-silicate multiplicity m. Two product analyses indicated by crosses and error bars (for discussion see text).

Conclusions

Synthetic anthophyllites accommodate large cations without losing overall long-range *Pnma* symmetry. Although our information on the mechanisms involved is still scanty, these appear to involve the development of large numbers of defects in the ideal amphibole structure.

We emphasize that in *structural* and *compositional* respects, the amphiboles synthesized here differ from the natural counterparts of which they were meant to be experimental analogs. As yet it is difficult to gauge the effects of these aberrations on the thermodynamic properties of the synthetic amphiboles, but the discrepancies need not be large to have profound effects on amphibole phase relations (*e.g.*, Day and Halbach, 1979).

A further complication is that natural amphiboles, besides being chemically more complex, themselves may also show varying degrees of structural disorder (*e.g.* Veblen, 1981). The focus of future experimental work involving amphibole must be to characterize in all respects synthetic products obtained, and to seek methods and techniques by which structural disorder and concomitant compositional inhomogeneity may be controlled in the experiment.

Acknowledgments

We are indebted to P. R. Buseck, H. W. Day, F. Liebau, W. Schreyer, F. Seifert, and especially D. R. Veblen for critical reviews as well as helpful comments and suggestions that helped clarify logic and presentation. We acknowledge that some of these reviewers prefer defect terminologies other than those used here. We also thank T. Baller for assistance in the laboratory, G. Werding for the chemical analyses, as well as O. Medenbach, A. Fricke, and K. Jochum for help with optical and X-ray determinations. The Kombat sample, in which tirodite was identified by the authors, was kindly provided by Herrn W. Kahn. Part of the research reported here was supported by grant Ma 689/2-1 of the Deutsche Forschungsgemeinschaft, Bonn.

References

Borg, I. Y., and Smith, D. K. (1969) Calculated X-ray powder patterns for silicate minerals. Geological Society of America Memoir 122.

Cameron, K. L. (1975) An experimental study of actinolite–cummingtonite phase relations with notes on the synthesis of Fe-rich anthophyllite. American Mineralogist, 60, 375–390.

Chernosky, J. V. Jr., and Autio, L. K. (1979) The stability of anthophyllite in the presence of quartz. American Mineralogist, 64, 294–303.

Czank, M., and Liebau, F. (1980) Periodicity faults in chain silicates: A new type of planar lattice fault observed with high-resolution electron microscopy. Physics and Chemistry of Minerals, 6, 85–93.

Dasgupta, H. C., Seifert, F., and Schreyer, W. (1974) Stability of mangano-cordierite and related phase equilibria in part of the system $MnO–Al_2O_3–SiO_2–H_2O$. Contributions to Mineralogy and Petrology, 43, 275–294.

Day, H. W., and Halbach, H. (1979) The stability field of anthophyllite: the effect of experimental uncertainty on per-

missible phase diagram topologies. American Mineralogist, 64, 809–823.

Evans, H. T. Jr., Appleman, D. E., and Handwerker, D. S. (1963) The least squares refinement of crystal unit cells with powder diffraction data by an automatic computer indexing method (abstr.). American Crystallographic Association Annual Meeting Program, 1963, 42–43.

Finger, L. W. (1970) Refinement of the crystal structure of an anthophyllite. Carnegie Institution of Washington Year Book, 68, 283–288.

Forbes, W. C. (1971) Synthesis of grunerite, $Fe_7Si_8O_{22}(OH)_2$. Nature Physical Sciences, 232, 109.

Gibbs, G. V. (1969) Crystal structure of protoamphibole. Mineralogical Society of America Special Paper 2, 101–109.

Greenwood, H. J. (1963) The synthesis and stability of anthophyllite. Journal of Petrology, 4, 317–351.

Hamilton, D. L. and Henderson, C. M. B. (1968) The preparation of silicate compositions by a gelling method. Mineralogical Magazine, 36, 832–838.

Hawthorne, F. C. (1981) Crystal chemistry of the amphiboles. In D. R. Veblen, Ed., Reviews in Mineralogy, Vol. 9A, p. 1–102. Mineralogical Society of America.

Hawthorne, F. C., Griep, J. L., and Curtis, L. (1980) A three-amphibole assemblage from the Tallan Lake sill, Peterborough County, Ontario. Canadian Mineralogist, 18, 275–284.

Hinrichsen, T. (1967) Über den Stabilitätsbereich der Mg–Fe^{2+}–Al-Mischkristallreihe rhombischer Hornblenden, Teil I: Hydrothermale Untersuchungen der Anthophyllit-Ferroanthophyllit-Mischkristallreihe. Neues Jahrbuch für Mineralogie Monatshefte, 257–270.

Hsu, L. C. (1968) Selected phase relationships in the system Al–Mn–Fe–Si–O–H: A model for garnet equilibria. Journal of Petrology, 9, 40–63.

Immega, I. P. and Klein, C., Jr. (1976) Mineralogy and petrology of some metamorphic Precambrian iron-formations in southwestern Montana. American Mineralogist, 61, 1117–1144.

Ito, J. (1972) Synthesis and crystal chemistry of Li-hydropyroxenoids. Mineralogical Journal (Tokyo), 7, 45–65.

Jaffe, H. W., Meijer, W. O. J. G., and Selchow, D. H. (1961) Manganoan cummingtonite from Nsuta, Ghana. American Mineralogist, 46, 642–653.

Johannes, W. and Schreyer, W. (1981) Experimental introduction of CO_2 and H_2O into Mg-cordierite. American Journal of Science, 281, 299–317.

Johannsen, K. (1930) Vergleichende Untersuchungen an Anthophyllit, Grammatit und Cummingtonit. Zeitschrift für Kristallographie, 73, 31–51.

Kisch, H. J. (1969) Magnesiocummingtonite-$P2_1/m$: A Ca- and Mn-poor clino-amphibole from New South Wales. Contributions to Mineralogy and Petrology, 21, 319–331.

Klein, C. Jr. (1964) Cummingtonite–grunerite series: a chemical, optical, and X-ray study. American Mineralogist, 49, 963–982.

Klein, C. Jr. (1966) Mineralogy and petrology of the metamorphosed Wabush iron formation, southwestern Labrador. Journal of Petrology, 7, 218–330.

Klein, C. Jr. and Waldbaum, D. R. (1967) X-ray crystallographic properties of the cummingtonite–grunerite series. Journal of Geology, 75, 379–392.

Leake, B. E. (1978) Nomenclature of amphiboles. Canadian Mineralogist, 16, 501–520.

Lindemann, W. (1964) Beitrag zur Struktur des Anthophyllits (abstr.). Fortschritte der Mineralogie, 42, 205.

Maresch, W. V. and Langer, K. (1976) Synthesis, lattice constants and OH-valence vibrations of an orthorhombic amphibole with excess OH in the system Li_2O–MgO–SiO_2–H_2O. Contributions to Mineralogy and Petrology, 56, 27–34.

Maresch, W. V., and Mottana, A. (1976) The pyroxmangite-rhodonite transformation for the $MnSiO_3$ composition. Contributions to Mineralogy and Petrology, 55, 69–79.

Papike, J. J., Ross, M., and Clark, J. R. (1969) Crystal chemical characterization of clinoamphiboles based on five new structure refinements. Mineralogical Society of America Special Paper 2, 117–136.

Peters, Tj., Valarelli, J. V., Coutinho, J. M. V., Sommerauer, J., and von Raumer, J. (1977) The manganese deposits of Buritirama (Pará, Brazil). Schweizerische Mineralogische und Petrographische Mitteilungen, 57, 313–327.

Popp, R. K., Gilbert, M. C., and Craig, J. R. (1976) Synthesis and X-ray properties of Fe–Mg orthoamphiboles. American Mineralogist, 61, 1267–1279.

Ravior, E. and Hinrichsen, Th. (1975) Upper stability of synthetic anthophyllite mixed crystals. Neues Jahrbuch für Mineralogie Monatshefte, 162–166.

Ross, M., Papike, J. J., and Shaw, K. W. (1969) Exsolution textures in amphiboles as indicators of subsolidus thermal histories. Mineralogical Society of America. Special Paper 2, 275–299.

Seifert, F., and Virgo, D. (1974) Temperature dependence of intracrystalline Fe^{2+}–Mg distribution in a natural anthophyllite. Carnegie Institution of Washington Year Book 73, 405–411.

Segeler, C. G. (1961) First U. S. occurrence of manganoan cummingtonite, tirodite. American Mineralogist, 46, 637–641.

Stephenson, N. C. N., and Hensel, H. D. (1979) Intergrown calcic and Fe–Mg amphiboles from the Wongwibinda Metamorphic Complex, NSW, Australia. Canadian Mineralogist, 17, 11–23.

Sueno, S., Papike, J. J., Prewitt, C. T., and Brown, G. E. (1972) Crystal structure of high cummingtonite. Journal of Geophysical Research, 77, 5767–5777.

Veblen, D. R. (1981) Non-classical pyriboles and polysomatic reactions in biopyriboles. In D. R. Veblen, Ed., Reviews in Mineralogy Vol. 9A, p. 189–236. Mineralogical Society of America.

Veblen, D. R. and Burnham, C. W. (1978a) New biopyriboles from Chester, Vermont: I. Descriptive mineralogy. American Mineralogist, 63, 1000–1009.

Veblen, D. R. and Burnham, C. W. (1978b) New biopyriboles from Chester, Vermont: II. The crystal chemistry of jimthompsonite, clinojimthompsonite, and chesterite, and the amphibole-mica reaction. American Mineralogist, 63, 1053–1073.

Veblen, D. R. and Buseck, P. R. (1979) Chain-width order and disorder in biopyriboles. American Mineralogist, 64, 687–700.

Veblen, D. R. and Buseck, P. R. (1981) Hydrous pyriboles and sheet silicates in pyroxenes and uralites: intergrowth microstructures and reaction mechanisms. American Mineralogist, 66, 1107–1134.

Wright, T. L. and Stewart, D. B. (1968) X-ray and optical study of alkali feldspar: I. Determination of composition and structural state from refined unit cell parameters and 2*V*. American Mineralogist, 53, 38–87.

Manuscript received, March 11, 1982;
accepted for publication, January 6, 1983.